ACS Sustainable Chemistry & Engineering

Letter

Cite This: ACS Sustainable Chem. Eng. 2018, 6, 15988−15994

pubs.acs.org/journal/ascecg

# Abnormal Grain Growth as a Method To Enhance the Thermoelectric Performance of Nb-Doped Strontium Titanate Ceramics

Alexander Tkach,[†] João Resende,[†] K. Venkata Saravanan,[†] Maria Elisabete Costa,[†] Pablo Diaz-Chao,[‡] Emmanuel Guilmeau,[‡] Olena Okhay,[†] and Paula M. Vilarinho*[,†]

[†]CICECO − Aveiro Institute of Materials, Department of Materials and Ceramic Engineering, University of Aveiro, 3810-193 Aveiro, Portugal

[‡]Laboratoire CRISMAT, UMR 6508, CNRS, ENSICAEN, 6 Boulevard du Maréchal Juin, 14050 Caen Cedex 04, France

Supporting Information

**ABSTRACT:** Driven by the need for high-temperature *n*-type thermoelectrics for energy-harvesting sectors, $SrTi_{0.8}Nb_{0.2}O_{3\pm\delta}$ ceramics are prepared here from powders with average particle sizes of 270 and 800 nm by the conventional sintering in air at 1450 °C and further in $H_2/N_2$ at 1400 °C. In contrast to coarse particle powders, the use of fine particle powders under these conditions leads to abnormal grain growth and thereby bimodal grain size distribution in $SrTi_{0.8}Nb_{0.2}O_{3\pm\delta}$ ceramics. As a result, a 3-fold increase in the thermoelectric figure of merit to 0.36 at 970 K is achieved, thus establishing the record value for bulk Nb-doped strontium titanate up to this temperature.

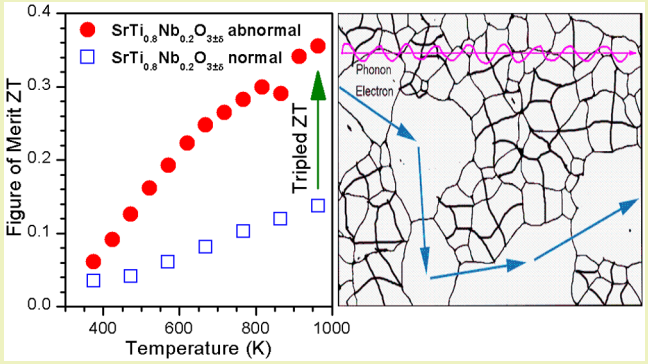


**KEYWORDS:** *Perovskite oxide electroceramics, Donor doping, Submicrometer particles, Two-step sintering, Microstructure engineering, Thermoelectric figure of merit*

## INTRODUCTION

The increasing need for clean, sustainable energy sources to meet the exponentially rising energy demands of the world has compelled researchers and scientists worldwide to look for new power generation strategies. The capture of unused heat in automotive exhaustion, industrial processes and home heating is one possible source of energy that is still unexploited. In the USA, wasted energy in the form of heat is close to 60% of the total energy produced.[1] The harvesting of this lost heat could improve significantly the system efficiency, reducing the electric supplying costs.[1] One of the potential devices to harvest the energy dissipated by heat is a thermoelectric (TE) generator, operating due to an existent gradient of temperature.[2] The operation system of this device is intrinsically related with the Seebeck effect present in a variety of materials, where an electrical response is caused by a difference of temperature trough itself or vice versa.[2]

The efficiency of the thermoelectric generator (TEG) depends on the material's figure of merit ($ZT$), which is a dimensionless quantity that relates different thermal and electrical properties $ZT = S^2 \cdot \sigma \cdot T/\kappa$, where $S$ is the Seebeck coefficient, $\sigma$ the electrical conductivity, $\kappa$ thermal conductivity, and $T$ the absolute average temperature of operation.[3]

Nevertheless, the high cost of production and materials, combined with modest energy conversion efficiency, made the application of TE generators only relevant in a limited field such as remote power generation for unmanned systems or radioisotope thermal generators for satellites.[3] In other areas such as space and vehicles wasted heat recovery has just been developed in the last years.[4] Additional problems related with the toxicity of these materials, reduced abundance of some compounds, stability at high temperatures, and heavy weight prevent the widespread use of this technology.[3] The use of oxides is a possible approach to solve some of the actual concerns of TEGs, reducing costs and weight, and permitting usage at high temperatures.[5]

Strontium titanate ($SrTiO_3$, ST), when carrier doped, is one of the versatile and most widely researched oxides for the *n*-type component of a TEG.[5,6] The carrier doping used to be performed by substitution of $Sr^{2+}$ with $La^{3+}$ on the A site[7,8] or $Ti^{4+}$ with $Nb^{5+}$ on the B site of an $ABO_3$ perovskite lattice[9−12] or both,[13,14] yielding a maximum $ZT$ of 0.41 at 973 K,[8] 0.35 at 1000 K,[9] and >0.6 at >1000 K,[13] respectively. The intrinsically high Seebeck coefficient, large electrical conductivity, and high

Received: August 12, 2018
Revised: October 5, 2018
Published: November 7, 2018






DOI: 10.1021/acssuschemeng.8b03875
ACS Sustainable Chem. Eng. 2018, 6, 15988−15994

melting temperatures are the fundamental properties of the ST-based systems for TE applications. Thus, the power factor ($S^2\sigma$) of doped ST is comparable to the conventional TE materials, whereas its $ZT$ is meager due to the large $\kappa$.[5]

Modifications of the grain size and nanostructuring have been theoretically reported to lower the value of $\kappa$.[15] An increase in the number of such interfaces as grain boundaries will increase the phonon scattering in the polycrystalline structure, leading to a decrease in the thermal conductivity.[5] Additionally, the reduction of the grain size will increase the scattering of the phonons with shorter mean free paths at the grain boundaries, creating a wider range of scattered phonons.[5] However, refining the grain sizes leads to an increase in the electrical resistivity, which is not favorable for enhancing the $ZT$ values.[16] To fully functionalize such dual effects of grain size, a high-performance TE material may need a combination of coarse and fine grains in an individual material, as was shown by Zhao et al. for $Bi_2Te_3$ thermoelectric material.[17] Then, electrical resistivity of the mixed grains may be kept almost unchanged if the connectivity of the coarse grains are not destroyed, but its thermal conductivity may be fairly reduced by the enhanced scattering effect in the fine grain areas because phonons do not "select" their path like electronic carriers. However, toxicity, scarcity, and high costs will hinder TE materials as $Bi_2Te_3$ to find universal application if their environmental impact will be considered.[18] Moreover, they are limited in their ability to harvest electricity at high temperatures, such as from solar and industrial waste heat, due to their decomposition and volatilization at elevated temperatures.[18] As a result, there is a need of new, low-cost, and environmentally friendly TE materials based on oxides despite the fact that generally oxides have low carrier mobility and high thermal conductivity. Within this context, we propose here the use of abnormal grain growth to obtain the required bimodal grain size distribution in ST-based oxide ceramics for the optimization of the TE figure of merit.

Indeed, bimodal grain size distribution in ceramics is usually related to the abnormal grain growth in the presence of a liquid phase, whereas the temperature range, where abnormal grain growth occurs, depends on the initial powder particle size, as was observed in ST ceramics with addition of 0.5 at. % of Nb.[19,20] In these ceramics prepared from 3-$\mu$m-sized powders, abnormal grain growth started at 1500 °C and was completed at 1540 °C. In ST ceramics prepared with 500-nm-sized powders, the onset and completion temperatures of abnormal grain growth decreased to 1460 and 1510 °C, respectively. Finally, for 300-nm-sized powders, the temperatures decreased further to 1445 and 1470 °C, respectively.[19,20] Therefore, assuming that such a trend can also be valid for $SrTi_{0.8}Nb_{0.2}O_{3\pm\delta}$ ceramics, we decided to prepare Nb-doped ST powders by a conventional mixed oxide method and separate them in coarse- and fine-particle-sized powders by centrifugation. Then, similarly to the fabrication of $BaTiO_3$ with millimeter-scale grains,[21] a two-step firing, consisting of sintering in air at 1450 °C for abnormal grain growth nucleation in fine-particle-sized ceramics, and further at 1400 °C for the growth of selected grains, was decided to be conducted. Thus, with this strategy, we intend to prove that the microstructural tuning of Nb-doped ST by powder morphology and a sintering cycle design in conventionally sintered ceramics can result in a high $ZT$ TE oxide of $n$-type.

## EXPERIMENTAL SECTION

Preparation of Nb-doped ST ceramics was divided into three main parts: powders preparation, adjustment of the particle size, and two-step sintering processes. These preparation steps affect the ceramics densities and grain size distribution. $SrTi_{0.8}Nb_{0.2}O_{3\pm\delta}$ (STN20) ceramics composition was prepared by a solid-state reaction of mixed powders with the accurate stoichiometry of $SrCO_3$ (Merck, 99%), $TiO_2$ (Sigma-Aldrich, 99%), and $Nb_2O_5$ (Alfa Aesar, 99.9%), although higher purity of $Nb_2O_5$ implies about 0.2 at. % excess of B site ions thus favoring the formation of a liquid phase and thereby promoting the abnormal grain growth in the particle size-dependent temperature range according to Bae et al.[19,20] The powders were mixed by ball milling in Teflon jars at 300 rpm for 5 h with zirconia balls in an ethanol medium. The calcination was performed for 2 h at 1200 °C with heating and cooling rates of 10 °C/min. The powders were again ball milled in Teflon jars at 300 rpm for 72 h in ethanol with a proportion of zirconia balls of 1:10. Coulter Multisizer (LS230, Beckman Coulter, Inc.) analysis revealed a double peak distribution of powder particle size after milling. For separation, powders were suspended in water with a concentration of 20 g/L, mixed in the ultrasounds for 5 min, and centrifuged for 1 min at 1000 rpm. The slurry and the precipitate were collected, filtered, and dried in order to obtain fine (~270 nm in average) and coarse (~800 nm in average) particles. Circular pellets of 10 mm in diameter and rectangular pellets of 15 mm × 5 mm of each of these two powders were uniaxially pressed at 20 MPa for 30 s, followed by cold isostatic pressing at 200 MPa for 15 min. The pellets were sintered in air at 1450 °C for 10 h and further in 10% $H_2$/90% $N_2$ reducing atmosphere at 1400 °C for 10 h with the heating and cooling rates of 10 °C/min. The sintering temperature of 1450 °C is within the abnormal grain growth temperature range for ~300-nm-sized powders but below that for above 300-nm-sized powders according to Bae et al.,[19,20] thus anticipating bimodal and unimodal grain size distribution for STN20 ceramics prepared from fine and coarse particle powders, respectively.

Structural and microstructural characterization was carried-out by X-ray diffraction (XRD), scanning electron microscopy (SEM), and optical microscopy. Density of sintered ceramics was measured by the Archimedes method, immersing the samples in ethylene glycol. Room temperature XRD analysis (Rigaku D/Max-B, Cu K$\alpha$) was conducted on ground sintered samples. The diffraction angle ($2\theta$) was in the range of 20°−80° with a sampling step of 0.02°. The lattice parameter was calculated by a least-squares-approach fitting of the XRD data using Rietveld refinement FullProf software. The microstructure of the ceramics was observed on polished and thermally etched at 1350 °C in a $H_2/N_2$ atmosphere for 1 min sections using SEM (Hitachi S-4100) and field emission SEM (Hitachi SU-70). Grain size distribution of ceramics is obtained using the Feret diameter determination method within the image analysis software ImageJ. The electrical resistance and Seebeck coefficient were measured on a commercial ZEM 3 device (ULVAC-RIKO) in a partial helium atmosphere. In order to obtain the thermal conductivity, the thermal diffusivity was measured using a Laser Flash technique (NETZSCH LFA 457 MicroFlash), while the specific heat was measured by differential scanning calorimetry (NETZSCH STA 449 F5 Jupiter) in argon. Then, thermal conductivity was calculated from the heat capacity ($C_p$), density ($\rho$), and thermal diffusivity ($\alpha$), according to the expression $\kappa = C_p \cdot \rho \cdot \alpha$. The estimated measurements uncertainties are 6% for the Seebeck coefficient, 8% for the electrical resistivity, 11% for the thermal conductivity, and 16% for the final figure of merit, $ZT$.[22]

## RESULTS AND DISCUSSION

The XRD profiles of the two-step-sintered Nb-doped ST ceramics are shown in Figure 1 in logarithmic scale. The observed X-ray diffraction lines are analogous for STN20 ceramics prepared from fine- and coarse-particle-sized powders, being also consistent with the cubic crystallographic structure of undoped ST. No distinct second phases are



DOI: 10.1021/acssuschemeng.8b03875
ACS Sustainable Chem. Eng. 2018, 6, 15988−15994

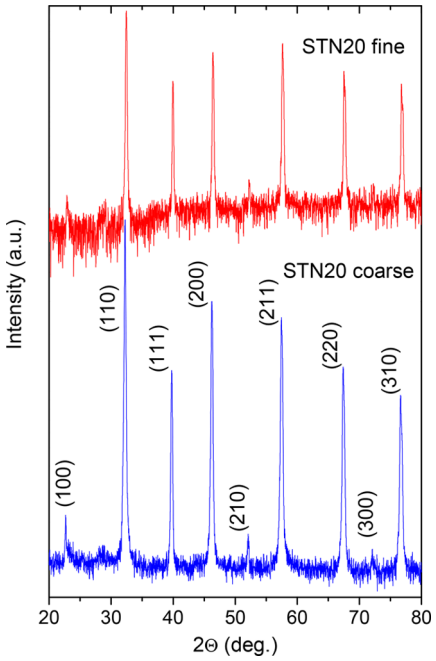


**Figure 1.** XRD profiles of fine- (top) and coarse- (bottom) particle-sized STN20 ceramics sintered in air at 1450 °C for 10 h and further in $H_2/N_2$ at 1400 °C for 10 h. Reflections of $SrTiO_3$ phase are marked by corresponding indexes.

detected, besides a small hill around 29° that is due to our XRD instrument. The lattice parameter deduced by Rietveld refinement of the XRD profiles of Nb-doped ST ceramics (Figure S1) is 393.33(1) pm that is close to the one for $SrTi_{0.8}Nb_{0.2}O_{3\pm\delta}$ directly sintered for 10 h in $H_2/N_2$ atmosphere at 1500 °C by Kovalevsky et al.[10] At the same time, the lattice parameter is much higher than 390.5 pm reported for undoped ST,[23] confirming the replacement of small-sized $Ti^{4+}$ ions (60.5 pm) with the larger $Nb^{5+}$ ions (64.0 pm).[24]

The SEM micrographs of STN20 ceramics prepared from coarse- and fine-particle-sized precursor powders are shown in Figure 2a and b, respectively. These ceramics undoubtedly present different microstructures, being however chemically homogeneous (Figure S2). The average grain size for the ceramics prepared from coarse-particle-sized powders (Figure 2a) is 8 $\mu$m. On the other hand, the chosen heat treatment of the fine-sized powder STN20 yields ceramics with an abnormal grain growth, as shown in Figure 2b and c. In this case, the grain size distribution is clearly bimodal as seen also from Figure 2d. Small grains are of 2.3 $\mu$m size in average, ranging from sub$\mu$m to ~5 $\mu$m (Figure 2c and d, left), whereas the average size for larger grains is around 59 $\mu$m, while the larger grain size distribution ranges from 10 to 120 $\mu$m (Figure 2b and d, right).

Thus, despite the difference in the Nb content and B site ions excess, the trend formerly observed in ST ceramics with the addition of 0.5 at. % of Nb[19,20] is indeed valid for our STN20 ceramics, and the abnormal grain growth was nucleated in our fine-particle-sized ceramics during the sintering in air at 1450 °C, being further developed during firing at 1400 °C. Such a two-step grain growth mechanism is called secondary abnormal grain growth and was reported to be successful in growth of millimeter-scale grains of $BaTiO_3$.[21] On the other hand, the firing temperatures used in our work were not enough to induce and support the abnormal grain growth in the coarse-sized STN20 ceramics, where the grains grew normally. At the same time, the ceramics density (and therefore the pores fraction) is almost independent of the precursor powders initial particle size variation, being 5.13 g/cm$^3$ (97.7% of theoretical density) for coarse-sized powder STN20 and 5.17 g/cm$^3$ (98.4%) for fine-sized powder STN20.

The analysis of the three TE properties (electrical conductivity, Seebeck coefficient, and thermal conductivity) is fundamental to evaluate the possible efficiency of TEG based on Nb-doped ST. The temperature dependence of the electrical conductivity ($\sigma$) is shown in Figure 3a, where a decreasing trend is observed for the uniform grain-sized microstructure of ceramics prepared from coarse particles in a whole measurement temperature range and for the nonuniform grain-sized microstructure of ceramics prepared from fine particle STN20 above 470 K in proportion to $T^{-1.5}$ and $T^{-1.8}$, respectively, indicating that phonon scattering was the dominant mechanism above that temperature.[9,25]

The initial increase in conduction with temperature for fine-particle-derived STN20 resembles that observed in electrical conductivity or charge carrier mobility for $SrTi_{0.8}Nb_{0.2}O_{3\pm\delta}$ fine-grained ceramics[11] and polycrystalline films[9] but not for coarse-grained ceramics or epitaxial films of the same composition.[9] The reduced carrier mobility at low temperatures was attributed to the structural distortion-induced localized states originated from doping and accelerated by the crystal size reduction.[11,25] Then, the semiconductor-like increase in the conductivity until the peak temperature suggests that the localized electrons can be thermally excited.[11] Accepting that microstructure affects mainly carrier mobility[9] and applying the localized states model to our case, we should mention as well that in our ceramics charge carrier concentration was also estimated from Hall effect measurements at room temperature using the Quantum Design Physical Properties Measurement System (PPMS) and found to be around $10^{21}$ cm$^{-3}$ for both samples, although the signal was not very linear and thereby the error was rather large due to an anomalous contribution, making it difficult to extract the reliable difference in the charge carrier concentration values. Thus, submicrometer grains observed in fine-sized powder STN20 (Figure 2c) and not seen in coarse-sized powder STN20 (Figure 2a) seem to trap the electrons reducing their mobility at low temperatures. However, when the localized electrons are thermally excited at high temperatures, the ceramics prepared with finer powders present higher values of conductivity compared to coarse-particle-derived ceramics because of the lower number of grain boundaries within the channels of the large connected grains. The highest value of electrical conductivity is 896 S/cm at 470 K, whereas at 970 K it reaches 328 S/cm, almost twice as high as that for ceramics produced with coarser powders. Moreover, it is about 1 order of magnitude higher than that for stoichiometric $SrTi_{0.8}Nb_{0.2}O_{3\pm\delta}$ ceramics directly sintered by Kovalevsky et al. for 10 h in $H_2/N_2$ atmosphere at 1500 °C.[10]

Figure 3b shows the temperature dependence of the Seebeck coefficient ($S$), which has negative values confirming that both samples are $n$-type materials. Ceramics produced with finer powders present more negative values of $S$, although the difference between the ceramics prepared from the two different precursor powders is only ~20 $\mu$V/K. Since the charge carrier concentration was estimated to be around $10^{21}$ cm$^{-3}$ for both samples while the ionized impurity scattering,


DOI: 10.1021/acssuschemeng.8b03875
ACS Sustainable Chem. Eng. 2018, 6, 15988−15994

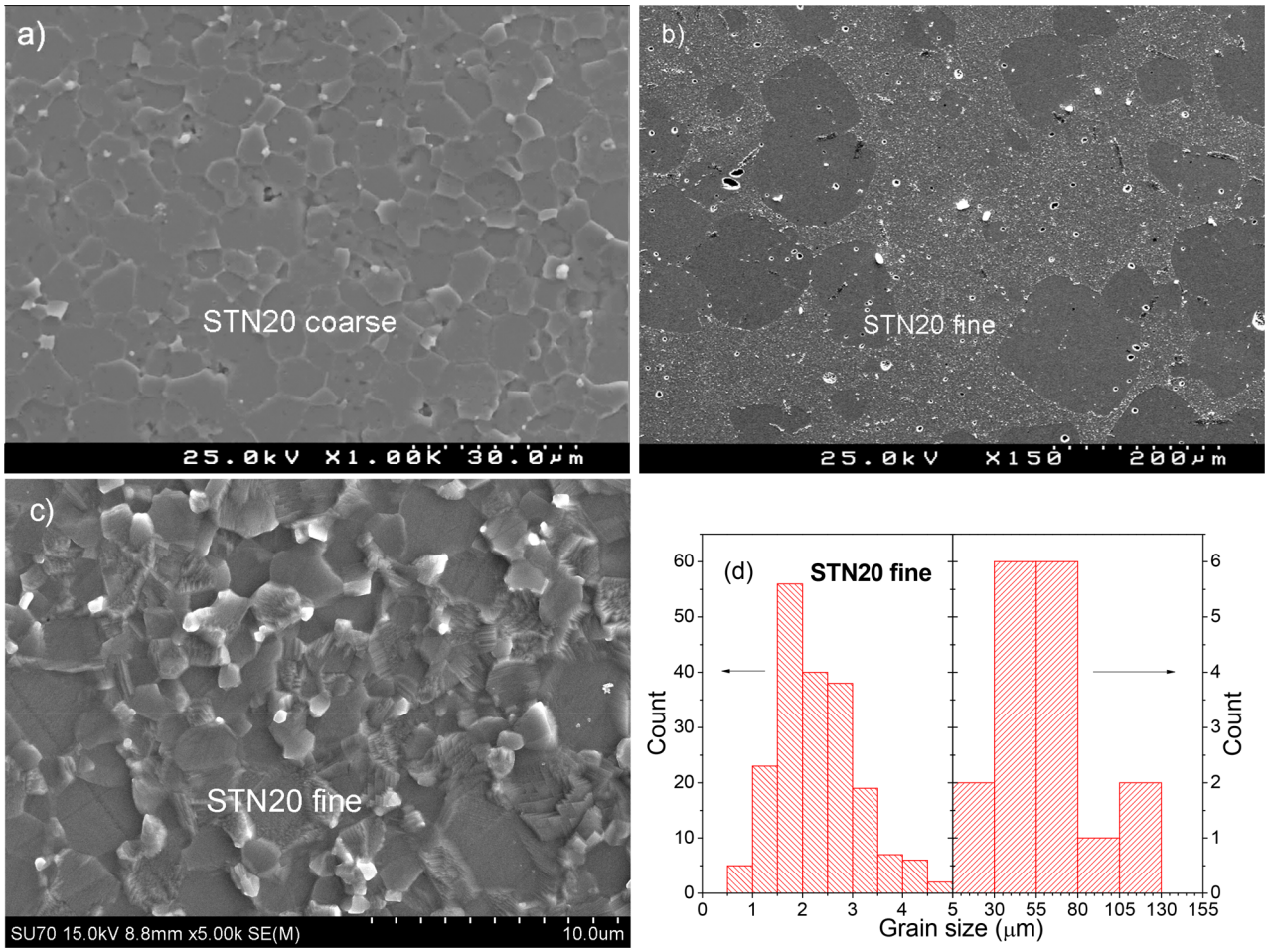


**Figure 2.** SEM micrographs of STN20 ceramics sintered from coarse- (a) and fine- (b,c) particle-sized powders at 1450 °C for 10 h in air and further at 1400 °C for 10 h in $H_2/N_2$, recorded with magnification of ×1000 (a), ×150 (b), and ×5000 (c). (d) Grain size distributions of fine-particle-derived STN20 ceramics, confirming the bimodal distribution, with an average grain size of 2.3 $\mu$m for the small grains (left scale) and 59 $\mu$m for the abnormal grains (right scale).

optical phonon scattering, and acoustic phonon scattering are independent of the grain size,[17] the enhanced $S$ should be related to the potential barrier scattering contribution[17] or energy filtering.[26] Indeed, potential (double Schottky) barriers are formed at the grain boundaries, but they should narrow dramatically in ST-based materials with increasing temperature.[9] Then, at low temperatures, the high energy carriers would overcome the potential barrier, whereas the low energy carriers would be stopped or strongly scattered by the potential barrier at the grain boundary, but at high temperatures both of them should be able to pass through the barrier. In our ceramics, however, we observe almost a temperature-independent difference in the Seebeck coefficient for coarse- and fine-particle-derived ceramics, indicating that energy filtering should be the main mechanism behind that behavior. Then, based on Figure 2b, we can assume that high conductivity channels constructed from large grains do not percolate across all the sample, possessing necks of micrometer and submicrometer grains, presented in Figure 2c, which perform energy filtering allowing high kinetic energy carriers to pass and stopping low energy ones, thus increasing the Seebeck coefficient in fine-particle-derived STN20. The magnitude of the Seebeck coefficient is in agreement with previous studies,[10,11] whereas the simultaneous increase in $\sigma$ and $S$ for fine-particle-derived ceramics resembles the higher Seebeck coefficient obtained by Ohta et al. on STN20 epitaxial films in comparison to STN20 ceramics despite higher carrier concentration and mobility values.[9]

Figure 3c shows the power factor ($S^2\sigma$) as a function of the temperature, obtained from the values of electrical conductivity and Seebeck coefficient. The power factor for fine-particle-derived STN20 ceramics reaches 13.4 $\mu$W/(K$^2$ cm) in the maximum, which is about 3 times higher than that of coarse-particle-derived ceramics. It is also higher than that reported for $SrTi_{0.8}Nb_{0.2}O_{3\pm\delta}$ ceramics before,[10,11] being comparable to that of $Bi_2Te_3$.[17] The increase in power factor is attributed to both the increase in electrical conductivity and the slight increase in Seebeck coefficient. That is in complete agreement with the results and model reported by Zhao et al.,[17] showing that bimodal grain size distribution enhances the thermoelectric performance of the material. However, in contrast to Zhao et al.,[17] who diluted coarse particles of ∼1 $\mu$m with fine ones of ∼100 nm, we have obtained the bimodal grain size distribution by abnormal grain growth of large grains in a matrix of small grains, using fine particle powders and two-step firing for the ceramics.

The thermal conductivity displays a decreasing trend with the temperature for both ceramics, as shown in Figure 4a. Moreover, the thermal conductivity values of coarse- and fine-particle-derived STN20 ceramics are rather similar at high


DOI: 10.1021/acssuschemeng.8b03875
ACS Sustainable Chem. Eng. 2018, 6, 15988−15994

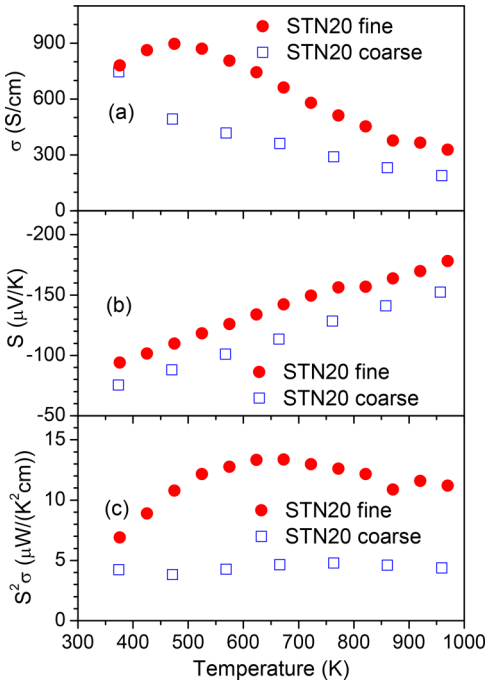


**Figure 3.** Electrical conductivity $\sigma$ (a), Seebeck coefficient $S$ (b), and power factor $S^2\sigma$ (c) of STN20 ceramics produced from coarse- (open squares) and fine- (solid circles) particle-sized powders versus temperature, showing up to 3-fold increase in power factor when fine particles are used.

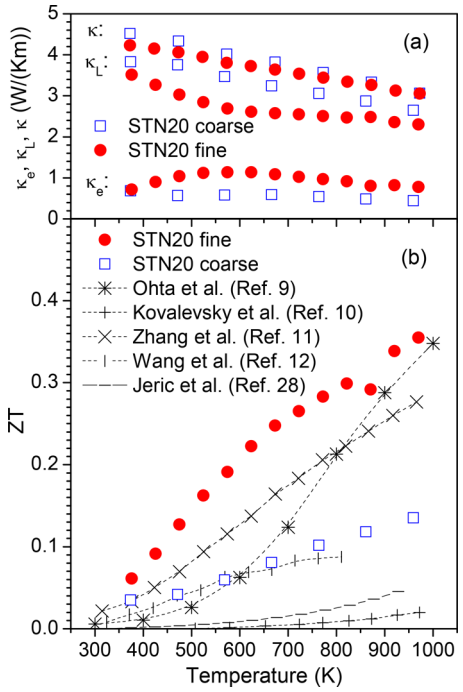


**Figure 4.** Thermal conductivity $\kappa$, its electronic $\kappa_e$, and lattice $\kappa_L$ components (a) and figure of merit $ZT$ (b) of STN20 ceramics produced from fine- (solid circles) and coarse- (open squares) particle-sized powders versus temperature. $ZT$ data for ceramics with identical composition from refs 9−12,28 are shown for comparison, demonstrating that STN20 ceramics with bimodal grain size distribution obtained in this work by conventional sintering possess the highest $ZT$ value of 0.36 at 970 K.

temperatures, although at low temperatures they are slightly smaller for the ceramics prepared from the fine particle sized powders. The lowest thermal conductivity value registered is of 3.06 W/(K m) at 970 K. The magnitude of the thermal conductivity is comparable to that reported for STN20 ceramics before,[9−12] particularly at high temperatures (Figure S3). The thermal conductivity is known to consist of electronic and lattice components $\kappa = \kappa_e + \kappa_L$, and electronic thermal conductivity can be estimated using the Wiedemann−Franz law $\kappa_e = L \cdot T \cdot \sigma$, where $L = (1.5 + \exp[-|S|/116]) \cdot 10^{-8}$ V$^2$/K$^2$ is the Lorenz number (Figure S4).[27] As shown in Figure 4a, the $\kappa_e$ contribution is up to 23% for fine-particle-derived STN20 and only ∼12% for coarse-particle-derived ceramics, implying that the $\kappa_L$ contribution is a dominant one. Moreover, it is evident that $\kappa_L$ is lowered for fineparticle-derived STN20.

The figure of merit, being directly connected with the potential efficiency of the material, relates all the other thermoelectric characteristics as $ZT = S^2 \cdot \sigma \cdot T/\kappa$. For both ceramics, $ZT$ increases with the temperature as presented in Figure 4b. In the case of coarse-particle-derived ceramics, it reaches 0.14 at 970 K. STN20 ceramics produced using the fine-particle-sized precursor powder reveal the highest $ZT$ value of 0.36 at 970 K obtained in this study.

For comparison purposes, previously reported data is also shown in Figure 4b. Ohta et al. reported $ZT$ value of 0.35 at 1000 K for ∼20-$\mu$m-grain-sized $SrTi_{0.8}Nb_{0.2}O_{3\pm\delta}$ ceramics hot pressed at 36 MPa and 1400 °C for 2 h, although on cooling toward room temperature $ZT$ diminished below 0.01.[9] Moreover, STN20 ceramics prepared using SPS by Wang et al. exhibited a maximum $ZT$ of ∼0.09 only at 823 K.[12] Zhang et al. prepared $SrTi_{0.8}Nb_{0.2}O_{3\pm\delta}$ powders by the hydrothermal method and sintered the ceramics at 1300 °C for 5 h, embedding them into carbon powder.[11] As a result, a $ZT$ of ∼0.28 at 970 K, increasing to ∼0.35 by lowering the Nb content to 10%, was reported.[11] However, such results could not be achieved, conventionally sintering the ceramics in a reducing atmosphere at 1500 °C.[10,28] Kovalevsky et al. could obtain $ZT$ for stoichiometric STN20 ceramics of ∼0.02 only at 970 K, increasing it to ∼0.23 by Sr deficiency,[10] while Jeric et al. reached a $ZT$ of 0.05 at 923 K, enhancing it to 0.08 by a CaO addition.[28] Thus, ceramics obtained in this work by a conventional route from powder with an average particle size of 270 nm, using sintering in air at 1450 °C for 10 h and further in $H_2/N_2$ at 1400 °C for 10 h that resulted in a bimodal grain size distribution, possesses the highest $ZT$ value of 0.36 at 970 K. This value is equal to that reported for La-doped ST with graphene inclusions at 1023 K[7] or for La- and Nb-codoped ST with Cu or Fe metallic nanoinclusions at 900 K[14] but is achieved in a simpler way of microstructure manipulation, not requesting fabrication and addition of the nanoinclusions.

## CONCLUSION

ST ceramics doped with 20% of Nb were produced using powders with average particle sizes of 270 and 800 nm aiming to enhance the thermoelectric performance by microstructural engineering. Coarse-particle-sized $SrTi_{0.8}Nb_{0.2}O_{3\pm\delta}$ ceramics obtained by the conventional sintering in air at 1450 °C and further in $H_2/N_2$ at 1400 °C present normal grain growth with average grain size of 8 $\mu$m, whereas those prepared from fine-particle-sized powders reveal abnormal grain growth with some grains reaching ∼59 $\mu$m in average and numerous grains



DOI: 10.1021/acssuschemeng.8b03875
ACS Sustainable Chem. Eng. 2018, 6, 15988−15994

growing to ~2 $\mu$m average size only. The origin of the bimodal grain size distribution is related with the fact that the abnormal grain growth temperature decreases for the smaller powder particle size as confirmed and used in this work. The large grains obtained in the fine-particle-derived $SrTi_{0.8}Nb_{0.20}O_{3\pm\delta}$ ceramics provide a conduction path for the electrons, thus substantially enhancing the electrical conductivity. At the same time, the thermal conductivity is lowered, since phonons have to propagate linearly across numerous small grains and their boundaries, being unable to "select" the path with minimum number of interfaces like charge carriers. As result, the *ZT* value is increased from 0.14 for conventionally prepared coarse-particle-derived $SrTi_{0.8}Nb_{0.2}O_{3\pm\delta}$ ceramics to 0.36 at 970 K for the fine-sized ceramics, establishing the latter value as the highest *ZT* ever reported for Nb-doped ST ceramics at this temperature. The results here obtained on donor-doped $SrTiO_3$ ceramics contribute to the fields of high-temperature thermoelectrics for the automotive and manufacturing energy-harvesting sectors and enhanced performance of *n*-type oxides. Finally, this approach can be extended to other prospective TE materials (chalcogenides, intermetallics, etc.) with the aim to synthesize a broad range of grain-size-controlled thermoelectrics with enhanced performances.

## ■ ASSOCIATED CONTENT

### Supporting Information

The Supporting Information is available free of charge on the ACS Publications website at DOI: 10.1021/acssuschemeng.8b03875.

XRD Rietveld refinement example, Lorenz numbers deduced from Seebeck coefficient data, SEM micrograph of fractured surface and EDS elemental mapping (Sr, Ti, and Nb) micrograph of strontium titanate ceramics doped with 20 at. % of Nb, as well as thermal conductivity comparison graph. (PDF)

## ■ AUTHOR INFORMATION


### Corresponding Author

*E-mail: paula.vilarinho@ua.pt.

### ORCID

Alexander Tkach: 0000-0002-0318-9262
Emmanuel Guilmeau: 0000-0001-7439-088X
Paula M. Vilarinho: 0000-0001-5161-1360


### Notes

The authors declare no competing financial interest.

## ■ ACKNOWLEDGMENTS

This work was developed within the scope of the project CICECO-Aveiro Institute of Materials, POCI-01-0145-FEDER-007679 (FCT ref. UID/CTM/50011/2013), financed by national funds through the FCT/MEC and when appropriate cofinanced by FEDER under the PT2020 Partnership Agreement as well as within FCT independent researcher grant IF/00602/2013. We thank Krzysztof Orlinski and Dorota A. Pawlak from the Institute of Electronic Materials Technology (ITME), Warsaw, Poland, for the heat capacity measurements.

## ■ REFERENCES


(1) Shakouri, A. Recent developments in semiconductor thermoelectric physics and materials. *Annu. Rev. Mater. Res.* **2011**, *41*, 399–431.
(2) MacDonald, D. K. C. *Thermoelectricity: An Introduction to the Principles*; Dover Publications, Mineola, NY, 2006.
(3) Vining, C. B. An inconvenient truth about thermoelectrics. *Nat. Mater.* **2009**, *8*, 83–85.
(4) Yang, J.; Caillat, T. Thermoelectric materials for space and automotive power generation. *MRS Bull.* **2006**, *31*, 224–229.
(5) Koumoto, K.; Wang, Y.; Zhang, R.; Kosuga, A.; Funahashi, R. Oxide thermoelectric materials: a nanostructuring approach. *Annu. Rev. Mater. Res.* **2010**, *40*, 363–394.
(6) Wang, H.; Su, W.; Liu, J.; Wang, C. Recent development of n-type perovskite thermoelectrics. *J. Materiomics.* **2016**, *2*, 225–236.
(7) Lin, Y.; Norman, C.; Srivastava, D.; Azough, F.; Wang, L.; Robbins, M.; Simpson, K.; Freer, R.; Kinloch, I. A. Thermoelectric Power Generation from Lanthanum Strontium Titanium Oxide at Room Temperature through the Addition of Graphene. *ACS Appl. Mater. Interfaces* **2015**, *7*, 15898–15908.
(8) Lu, Z.; Zhang, H.; Lei, W.; Sinclair, D. C.; Reaney, I. M. High-Figure-of-Merit Thermoelectric La-Doped A-Site-Deficient $SrTiO_3$ Ceramics. *Chem. Mater.* **2016**, *28*, 925–935.
(9) Ohta, S.; Ohta, H.; Koumoto, K. Grain size dependence of thermoelectric performance of Nb-doped $SrTiO_3$ polycrystals. *J. Ceram. Soc. Jpn.* **2006**, *114*, 102–105.
(10) Kovalevsky, A. V.; Yaremchenko, A. A.; Populoh, S.; Weidenkaff, A.; Frade, J. R. Effect of A-Site Cation Deficiency on the Thermoelectric Performance of Donor-Substituted Strontium Titanate. *J. Phys. Chem. C* **2014**, *118*, 4596–4606.
(11) Zhang, B.; Wang, J.; Zou, T.; Zhang, S.; Yaer, X.; Ding, N.; Liu, C.; Miao, L.; Li, Y.; Wu, Y. High thermoelectric performance of Nb-doped $SrTiO_3$ bulk materials with different doping levels. *J. Mater. Chem. C* **2015**, *3*, 11406–11411.
(12) Wang, J.; Ye, X.; Yaer, X.; Zhang, B.; Ma, W.; Miao, L. High thermoelectric performance of niobium-doped strontium titanate bulk material affected by all-scale grain boundary and inclusions. *Scr. Mater.* **2015**, *99*, 25–28.
(13) Wang, J.; Zhang, B.-Y.; Kang, H.-J.; Li, Y.; Yaer, X.; Li, J.-F.; Tan, Q.; Zhang, S.; Fan, G.-H.; Liu, C.-Y.; Miao, L.; Nan, D.; Wang, T.-M.; Zhao, L.-D. Record high thermoelectric performance in bulk $SrTiO_3$ via nano-scale modulation doping. *Nano Energy* **2017**, *35*, 387–395.
(14) Srivastava, D.; Norman, C.; Azough, F.; Schafer, M. C.; Guilmeau, E.; Freer, R. Improving the thermoelectric properties of $SrTiO_3$-based ceramics with metallic inclusions. *J. Alloys Compd.* **2018**, *731*, 723–730.
(15) Ohta, H.; Kim, S.; Mune, Y.; Mizoguchi, T.; Nomura, K.; Ohta, S.; Nomura, T.; Nakanishi, Y.; Ikuhara, Y.; Hirano, M.; Hosono, H.; Koumoto, K. Giant thermoelectric Seebeck coefficient of a two-dimensional electron gas in $SrTiO_3$. *Nat. Mater.* **2007**, *6*, 129–134.
(16) Slack, G. A.; Hussain, M. A. The maximum possible conversion efficiency of silicon-germanium thermoelectric generators. *J. Appl. Phys.* **1991**, *70*, 2694–2718.
(17) Zhao, L.-D.; Zhang, B.-P.; Liu, W.-S.; Li, J.-F. Effect of mixed grain sizes on thermoelectric performance of $Bi_2Te_3$ compound. *J. Appl. Phys.* **2009**, *105*, 023704.
(18) Koumoto, K.; Funahashi, R.; Guilmeau, E.; Miyazaki, Y.; Weidenkaff, A.; Wang, Y. F.; Wan, C. L. Thermoelectric Ceramics for Energy Harvesting. *J. Am. Ceram. Soc.* **2013**, *96*, 1–23.
(19) Bae, C.; Park, J.-G.; Kim, Y.-H. Effect of Powder Characteristics on the Microstructure and Electrical Property of Nb-doped $SrTiO_3$. *J. Kor. Phys. Soc.* **1998**, *32*, S296–S298.
(20) Bae, C.; Park, J.-G.; Kim, Y.-H.; Jeon, H. Abnormal Grain Growth of Niobium-Doped Strontium Titanate Ceramics. *J. Am. Ceram. Soc.* **1998**, *81*, 3005–3009.
(21) Lee, H.-Y.; Kim, J.-S.; Kim, D.-Y. Fabrication of $BaTiO_3$ single crystals using secondary abnormal grain growth. *J. Eur. Ceram. Soc.* **2000**, *20*, 1595–1597.




DOI: 10.1021/acssuschemeng.8b03875
*ACS Sustainable Chem. Eng.* 2018, 6, 15988–15994

(22) Alleno, E.; Bérardan, D.; Byl, C.; Candolfi, C.; Daou, R.; Decourt, R.; Guilmeau, E.; Hébert, S.; et al. Invited Article: A round robin test of the uncertainty on the measurement of the thermoelectric dimensionless figure of merit of $Co_{0.97}Ni_{0.03}Sb_3$. *Rev. Sci. Instrum.* **2015**, *86*, 011301.
(23) Mitsui, T.; Westphal, W. B. Dielectric and X-Ray Studies of $Ca_xBa_{1-x}TiO_3$ and $Ca_xSr_{1-x}TiO_3$. *Phys. Rev.* **1961**, *124*, 1354−1359.
(24) Shannon, R. D. Revised effective ionic radii and systematic studies of interatomic distances in halides and chalcogenides. *Acta Crystallogr., Sect. A: Cryst. Phys., Diffr., Theor. Gen. Crystallogr.* **1976**, *32*, 751−767.
(25) Park, K.; Son, J. S.; Woo, S. I.; Shin, K.; Oh, M.-W.; Park, S.-D.; Hyeon, T. Colloidal synthesis and thermoelectric properties of La-doped $SrTiO_3$ nanoparticles. *J. Mater. Chem. A* **2014**, *2*, 4217−4224.
(26) Berland, K.; Song, X.; Carvalho, P. A.; Persson, C.; Finstad, T. G.; Lovvik, O. M. Enhancement of thermoelectric properties by energy filtering: Theoretical potential and experimental reality in nanostructured ZnSb. *J. Appl. Phys.* **2016**, *119*, 125103.
(27) Kim, H. S.; Gibbs, Z. M.; Tang, Y.; Wang, H.; Snyder, G. J. Characterization of Lorenz number with Seebeck coefficient measurement. *APL Mater.* **2015**, *3*, 041506.
(28) Jeric, M.; de Boor, J.; Zavasnik, J.; Ceh, M. Lowering the thermal conductivity of $Sr(Ti_{0.8}Nb_{0.2})O_3$ by SrO and CaO doping: microstructure and thermoelectric properties. *J. Mater. Sci.* **2016**, *51*, 7660−7668.



DOI: 10.1021/acssuschemeng.8b03875
*ACS Sustainable Chem. Eng.* 2018, 6, 15988−15994